Draft version October 13, 2009
Preprint typeset using LaTeX style emulateapj v. 08/22/09

MG II ABSORPTION CHARACTERISTICS OF A VOLUME-LIMITED SAMPLE OF GALAXIES AT Z $\sim$ 0.1[1]

Elizabeth J. Barton[2] and Jeff Cooke[2,3]

Draft version October 13, 2009

ABSTRACT

We present an initial survey of Mg II absorption characteristics in the halos of a carefully constructed, volume-limited subsample of galaxies embedded in the spectroscopic part of the Sloan Digital Sky Survey. We observed quasars near sightlines to 20 low-redshift ($z \sim 0.1$), luminous ($M_r + 5 \log h \leq -20.5$) galaxies in SDSS DR4 and DR6 with the LRIS-B spectrograph on the Keck I telescope. The primary systematic criteria for the targeted galaxies are a redshift $z \gtrsim 0.1$ and the presence of an appropriate bright background quasar within a projected 75 h^{-1} kpc of its center, although we preferentially sample galaxies with lower impact parameters and slightly more star formation within this range. Of the observed systems, six exhibit strong [$W_{eq}(2796) \geq 0.3$ Å] Mg II absorption at the galaxy's redshift, six systems have upper limits which preclude strong Mg II absorption, while the remaining observations rule out very strong [$W_{eq}(2796) \geq 1 - 2$ Å] absorption. The absorbers fall at higher impact parameters than many non-absorber sightlines, indicating a covering fraction $f_c \lesssim 0.4$ for ≥ 0.3 Å absorbers at $z \sim 0.1$, even at impact parameters $\leq$35 h^{-1} kpc ($f_c \sim 0.25$). The data are consistent with a possible dependence of covering fraction and/or absorption halo size on the environment or star-forming properties of the central galaxy.

Subject headings: galaxies: evolution — galaxies: ISM — quasars: absorption lines

1. INTRODUCTION

Because gas consumption timescales in galaxies are short, massive galaxies must have large reservoirs of gas in order to fuel star formation throughout cosmic time. These reservoirs are likely quite diffuse and extended, and are therefore difficult to probe directly. Absorption lines in background quasars near galaxy sightlines allow a unique probe of this gas (e.g., Bergeron & Boissé 1991; Steidel & Sargent 1992; Steidel et al. 1994; Steidel 1995; Chen et al. 2001, and many more).

Absorption-line studies in transitions like Mg II have revealed a wealth of information about the absorbing gas and its relationship to galaxies (e.g., Bergeron & Boissé 1991; Steidel et al. 1994; Churchill et al. 1996; Nestor et al. 2005; Zibetti et al. 2005; Nestor et al. 2006, 2007; Zibetti et al. 2007). These results suggest that many — if not all — luminous intermediate-redshift galaxies are surrounded by Mg II-enriched gas that extends out to at least $\sim$40 h^{-1} kpc for luminous systems ($\sim$ 42 h^{-1} kpc if $\Omega_\Lambda = 0.7$; Steidel 1995) and likely much further in some cases (Churchill et al. 2005; Kacprzak et al. 2008). Estimates of the covering fractions of these gaseous halos range from $0.17 < f_c \leq 1$ (Steidel 1995; Bechtold & Ellingson 1992; Bowen et al. 1995; Kacprzak et al. 2008) in "strong" [$W_{eq}(2796) > 0.3\mathring{A}$] absorption systems. This threshold for strong absorbers is common and physically based; strong systems differ in character from weaker systems, which have higher covering fractions and different kinematics (Churchill et al. 1999, 2005; Nestor et al. 2005, 2006).

If gaseous halos around galaxies are reservoirs for star formation (Maller & Bullock 2004), the observed properties of galaxies likely depend on whether their gas halos are intact. Processes that may inhibit star formation in satellite galaxies include "strangulation," where the outer hot gas halo of a satellite galaxy is removed by the surrounding environment (e.g., Larson et al. 1980; Kawata & Mulchaey 2008). This removal prevents the further infall of cool gas. A more violent and immediate process is ram pressure stripping, which acts to remove cold, star-forming gas from galaxies, possibly quenching star formation soon after infall (e.g., Gunn & Gott 1972; Moore et al. 1996). These processes likely play a role in the observed environmental dependence of galaxy properties like color and morphology (e.g., Gunn & Gott 1972; Dressler 1980; Postman & Geller 1984; Blanton et al. 2005a). If stripping of the outer gas reservoir does regulate star formation, we might expect to find correlations between the properties of the galaxies and those of their halos. Many Mg II studies find dependence on galaxy luminosity or halo mass (e.g., Steidel et al. 1994; Bouché et al. 2006). Recently, Kacprzak et al. (2007) have shown that stronger absorbers also preferentially reside in asymmetric galaxies. Many early studies did not reveal trends with galaxy color or star-forming properties (Steidel et al. 1994; Guillemin & Bergeron 1997), although at least one study suggested that trends are possible (Bowen et al. 1995).

More recently, Zibetti et al. (2007) study a sample of nearly 3000 Mg II systems with $W_{eq}(2796) > 0.8$ Å at $0.37 < z < 1$ by using image-stacking techniques to probe the amount, spatial distribution, and colors of the integrated galaxian light from the multiple, stacked absorbers. Their results demonstrate that Mg II absorption is color dependent: the integrated galaxian light is

[1] The data presented herein were obtained at the W.M. Keck Observatory, which is operated as a scientific partnership among the California Institute of Technology, the University of California and the National Aeronautics and Space Administration. The Observatory was made possible by the generous financial support of the W.M. Keck Foundation.

[2] Center for Cosmology, Department of Physics and Astronomy, University of California, Irvine, CA 92697-4575; ebarton@uci.edu, cooke@uci.edu

[3] Gary McCue Postdoctoral Fellow

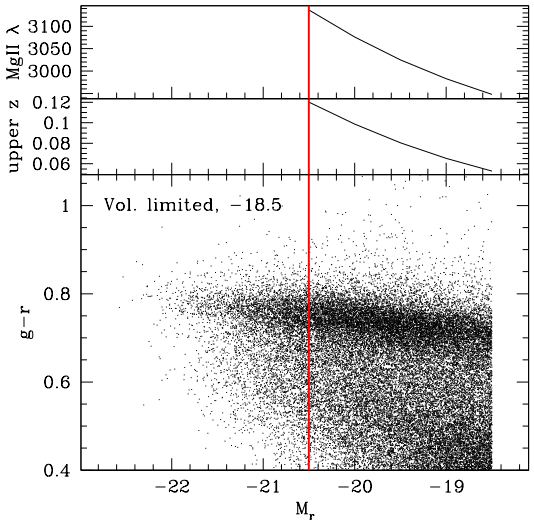

FIG. 1.— Constructing a volume-limited sample of galaxies to probe for halo Mg II absorption. We illustrate the challenge inherent in the use of SDSS to construct a sample for ground-based observations of haloMg II absorption. (*Bottom*) We show the color-magnitude distribution of a volume-limited sample to -18.5, showing both red and blue galaxies; observing as faint as possible is desirable to sample the blue cloud. As a function of absolute r-band magnitude limit chosen from the SDSS, we show the upper redshift limit (*Middle*) and the expected Mg II absorption wavelength (*Top*). As we demonstrate in this study, wavelengths above ∼3050 are largely accessible from the ground, suggesting that volume-limited samples from SDSS with limits in the range of $\lesssim -21$ to -20 are possible to probe. Here, we focus on the $M_r + 5\log h \lesssim -20.5$ sample.

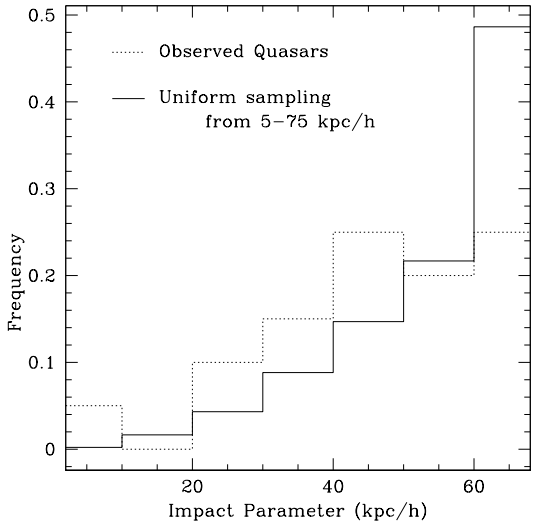

FIG. 2.— Distribution of impact parameters probed in the study (*Dotted line*) compared to a uniform distribution from 5-75 h^{-1} kpc. The sample is deficient in galaxies with impact parameters above $\sim 50 h^{-1}$ kpc ($P_{K-S} = 0.01$).

bluer for stronger absorbers and for galaxies that are closer to the quasar probes. However, these results are aggregate and are luminosity-weighted; it is difficult to disentangle the possible effects that result if, say, Mg II absorption is more common in lower-luminosity blue galaxies. Thus, while their creative statistical method has proven extremely powerful, it cannot reveal a one-to-one relationship that may exist between galaxy and Mg II properties.

Most of our knowledge of Mg II absorbers comes from redshifts $\gtrsim$ 0.4, where the Mg II doublet (λ 2796.35,2803.53 Å) is redshifted into the optical. Systems in lower-redshift galaxies are difficult to observe from the ground and, as a result, have not been studied as extensively. To date, detections indicate that the absorber abundances and covering fractions decline somewhat. Depending on their $W_{eq}(2796)$, the decline is not necessarily dramatic as redshifts approach zero (Bowen et al. 1995; Nestor et al. 2005, 2006).

The vast majority of existing Mg II studies of individual absorber-galaxy associations begin with quasar spectra and then use photometric or spectroscopic redshifts to identify the nearby galaxies responsible for the Mg II absorption (e.g., Bergeron & Boissé 1991; Steidel et al. 1994; Churchill et al. 1999, and many others). Studies that begin with quasar spectra frequently focus on galaxies already known to have Mg II absorption. Some also tabulate galaxies that clearly lack absorption, but Churchill et al. (2005) note that focused "control" studies are biased toward quasars near non-absorbers, or absorbers with patchier Mg II-absorbing gas. As Tripp & Bowen (2005) point out, "reversing" the problem by identifying a controlled galaxy sample first, and then finding a subset with background quasars, alleviates significant selection effects. Bowen et al. (1995) present a Hubble Space Telescope study of very nearby galaxies and Tripp & Bowen (2005) present preliminary results from a "reverse" study at $z \sim 0.2$ using galaxies selected photometrically from the SDSS.

Here, we present a "reverse" study from a well-defined, volume-limited spectroscopic sample of ∼L* galaxies from the Sloan Digital Sky Survey (SDSS). Their basic properties, such as environment, star-formation, and metallicity, can be placed into the very well-defined context of the SDSS. In § 2 we describe our sample selection and observational approach, and present the data. § 3 contains an analysis of our results, and we conclude in § 4.

2. SAMPLE SELECTION AND DATA REDUCTION

Our observations were designed to probe for the presence or absence of Mg II absorption from the ground in a well-understood, volume-limited *spectroscopic* survey of ∼L* galaxies at $z \sim 0.11$, selected with the fewest biases possible. The choice of limiting absolute magnitude for the sample is informed by: (1) the need to observe the strong [$W_{eq}(2796) > 0.3$ Å] Mg II lines as far above the atmospheric cutoff as possible, and (2) the desire to include lower luminosity galaxies, thus sampling both the red sequence and the blue cloud.

We illustrate the relationships between Mg II wavelength, the upper redshift limit, and the magnitude limit of a volume-limited sample from SDSS in Fig. 1. At $z \sim 0.1$, substantial contributions to the blue cloud extend to roughly absolute magnitudes of $M_r + 5\log h \gtrsim -21$ (e.g., Blanton et al. 2003). A volume-limited sample fainter than $M_r + 5\log h \sim -20$ has an upper redshift limit at which Mg II is well below the atmospheric cutoff. Thus, after exploring the available quasars in the SDSS DR5 quasar catalog (Schneider et al. 2007), we focus on a limiting magnitude of $M_r + 5\log h \lesssim -20.5$, yielding a volume-limited sample with enough quasar-galaxy pairs

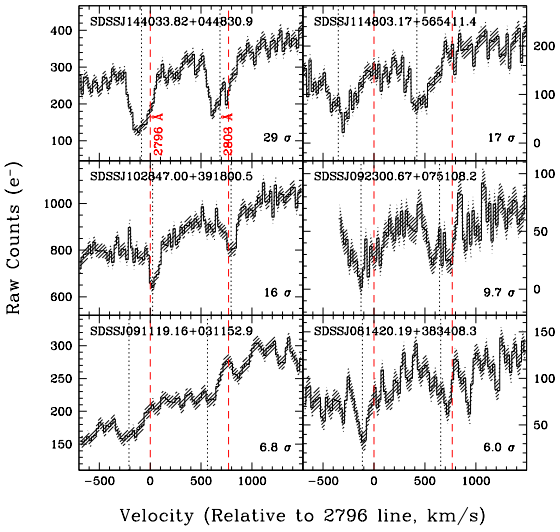

FIG. 3.— The detections. We plot raw object counts in detected electrons as a function of effective rest-frame (peculiar) velocity shift from the centroid of the 2796 Å line. The shading indicates the errors and vertical lines (*Dashed, red*) indicate the expected positions of the MgII lines from the galaxies if they occur at the redshift centroid; thinner (*dotted*) lines indicate the velocity offset of the maximum detection signal. We list the quasar name in the upper left, and the significance of the detection in the lower right. The bottom two spectra are box-car smoothed by 4 and 2 bins, respectively.

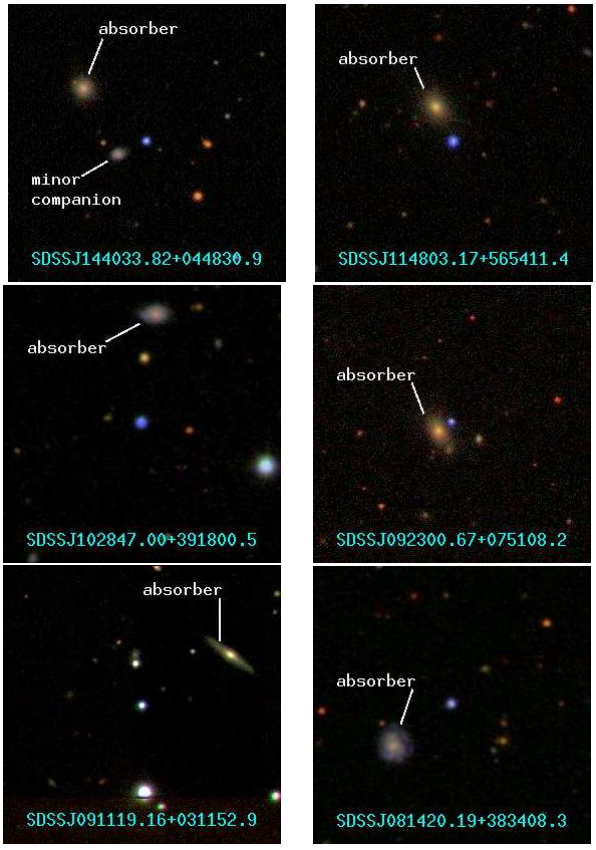

FIG. 4.— The detected galaxies. We show SDSS images of the quasars and likely absorbers. The central object is the quasar, and the images are 40″ on a side, corresponding (*Left to right*) to 58, 54, 58, 54, 50, and 51 h^{-1} kpc, respectively.

at $z \gtrsim 0.11$. This study is possible from the ground only with an optimally blue-sensitive spectrograph like the Low-Resolution Imaging Spectrometer-Blue channel (LRIS-B Oke et al. 1995; McCarthy et al. 1998). Few previous studies of this nature have been conducted because the low spectroscopic redshifts preclude ground-based observation of Mg II.

All but one of our targets originate from a volume-limited subsample of the SDSS DR6 NYU Value-Added Galaxy Catalog (NYU-VAGC) (Adelman-McCarthy et al. 2008; Blanton et al. 2005b). The volume-limited galaxy subsample constructed to $M_r + 5\log h \gtrsim -20.5$ includes 88,532 galaxies with redshifts $0.0044 \leq z \leq 0.116476$. The colors and magnitudes we quote are k-corrected and Galactic reddening corrected (Blanton et al. 2005b); spectral line information comes from the SpecLine data distributed via the SDSS web site. We ultimately select quasars at projected distances of $D \leq 75$ h^{-1} kpc in the SDSS DR5 quasar catalog. The quasars satisfy $m_g \leq 19.5$, with redshifts at which the observed-frame Lyman α emission from the quasar is blueward of the expected Mg II (2796 Å) absorption of the galaxy, allowing us to avoid contamination in the quasar spectrum from intervening Lyman α forest systems. We observed a total of 20 quasar-galaxy pairings. The signal-to-noise ratios of the resulting observations vary depending on the seeing conditions, the absorber redshift, and the flux of the quasar, as we describe below.

Our observations began with a pilot study that sampled the SDSS VAGC DR4 (Adelman-McCarthy et al. 2006), with a magnitude limit that extended to $M_r + 5\log h \leq -20$. Because the lower-redshift systems were more difficult to target than expected, we eventually focused on the -20.5 sample and extended the study to DR6. After the detection of an Mg II absorber system at an impact parameter of 62 h^{-1} kpc, we extended our impact parameter radius from 65 to 75 h^{-1} kpc. As Fig. 2 shows and a K-S test suggests, the sample is deficient in galaxies with impact parameters $\gtrsim 50$ h^{-1} kpc ($P_{K-S} \sim 0.01$).

The targets are listed in Table 1; only galaxy SDSSJ030313.02-001457.4 is missing from the DR6 database, for reasons that are unclear. As a result, we analyze all the spectra in the context of the SDSS VAGC DR6 $M_r + 5\log h \leq -20.5$ sample, referred to as the DR6 -20.5 sample hereafter.

2.1. *The Observational approach and the data*

We conducted observations on 2008 March 2 and 2009 January 24-25 using the 1200 l mm^{-1} grism blazed at 3400 Å with LRIS B; the longslit spectra approximately cover the wavelength range 2910 – 3890 Å. The objects for which we use slitmasks cover a similar area, sometimes beginning just redward of 3000 Å. The grism has good blue sensitivity, with an efficiency that remains high even shortward of 3100 Å. Its dispersion is 0.24 Å per pixel, which yields a ∼1.6 Å resolution with our 1.″0 slit and allows us to resolve the λ2796, 2803 Å doublet easily. We took 1-3 exposures for total on-source integration times of 1800 – 3600 seconds, depending on the magnitude of the quasar and the conditions during the night. We compute sensitivity limits that reflect these changing conditions on an object-by-object basis. We follow standard data reduction and extraction techniques. Because

Table 1. Basic Properties of Targeted SDSS Galaxies

QSO Name	Galaxy Position (2000)	Galaxy z	D (kpc/h)	QSO m_g	Galaxy M_R	Galaxy m_r	t_{exp} (sec.)	Sample Note
SDSSJ030313.02-001457.4	$03^h\ 03^m\ 13.27^s\ 00°\ 14'\ 20.5''$	0.1049	50	18.40	-21.38	16.38	3600	DR4 only
SDSSJ080409.23+385348.8	08 04 11.10 38 53 17.8	0.0979	48	17.84	-21.21	16.36	1800	
SDSSJ080814.69+475244.6	08 08 13.79 47 51 53.8	0.1094	71	17.89	-20.55	17.31	1800	
SDSSJ081420.19+383408.3	08 14 21.97 38 33 49.2	0.0978	35	18.06	-20.89	16.67	3600	
SDSSJ081940.82+443649.6	08 19 38.29 44 36 27.0	0.1116	49	19.05	-20.68	17.27	2700	
SDSSJ090558.34+504538.0	09 05 55.34 50 45 16.4	0.1062	48	18.04	-21.06	16.70	1800	
SDSSJ091119.16+031152.9	09 11 16.76 03 12 10.7	0.0963	50	17.43	-20.79	16.75	3600	
SDSSJ092300.67+075108.2	09 23 01.04 07 51 05.1	0.1039	8	18.51	-21.33	16.43	3600	
SDSSJ102216.13+621836.7	10 22 17.72 62 19 07.8	0.1162	48	19.34	-20.66	17.28	2400	
SDSSJ102751.62+104532.6	10 27 49.99 10 46 05.2	0.1093	56	18.58	-21.28	16.58	3600	
SDSSJ102847.00+391800.5	10 28 46.44 39 18 43.0	0.1135	62	17.09	-20.87	17.06	1800	
SDSSJ104706.74+375315.4	10 47 06.24 37 52 25.8	0.1018	65	18.74	-20.80	16.86	3300	
SDSSJ105033.08-001354.8	10 50 30.79 00 13 33.0	0.1155	59	18.81	-21.35	16.63	3600	
SDSSJ111342.42-000730.7	11 13 42.52 00 07 55.6	0.1094	34	19.10	-21.70	16.18	3600	
SDSSJ112613.52+352002.6	11 26 09.80 35 19 47.2	0.1117	68	17.79	-20.88	17.03	3600	DR6 only
SDSSJ114803.17+565411.4	11 48 03.81 56 54 25.6	0.1046	20	17.73	-21.28	16.49	3000	
SDSSJ124914.11+392615.0	12 49 17.42 39 26 33.3	0.1133	60	18.69	-20.63	17.27	3300	DR6 only
SDSSJ140843.77+004730.4	14 08 42.24 00 47 35.0	0.1146	34	19.21	-20.63	17.38	1800	
SDSSJ144033.82+044830.9	14 40 35.55 04 48 50.4	0.1129	46[a]	18.52	-21.03	16.90	1800	
SDSSJ151541.23+334739.4	15 15 40.76 33 47 52.3	0.1156	20	18.57	-20.59	17.39	1800	

TABLE 1
PROPERTIES OF OBSERVATIONS: (1) SDSS NAME OF QUASAR, (2) POSITION OF THE TARGETED GALAXY, (3) REDSHIFT OF TARGETED GALAXY, (4) IMPACT PARAMETER, OR PROJECTED ON-SKY DISTANCE BETWEEN QUASAR AND CENTER OF TARGETED GALAXY, (5) SDSS g-BAND MAGNITUDE OF QUASAR, (6) AND (7), ABSOLUTE AND APPARENT r-BAND MAGNITUDES OF THE TARGETED GALAXY, (8) TOTAL EXPOSURE TIME ON QUASAR, AND (9) COMMENTS ON SAMPLE MEMBERSHIP FOR TARGETED GALAXY.

[a]As noted in the text, there is a fainter companion galaxy (m_r = 18.1) with a coincident redshift (z = 0.1128) at $14^h\ 40^m\ 34.6^s$ $+04°\ 48'\ 25''$, a projected distance of only $\sim$ 18.6 h^{-1} kpc from the quasar.

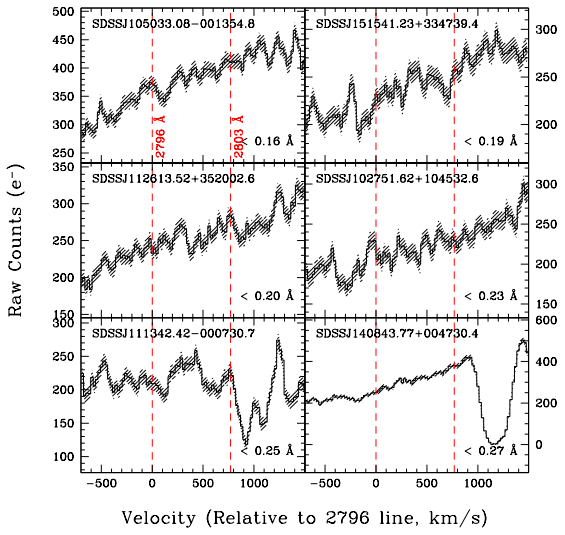

FIG. 5.— The solid non-detections of $\geq$ 0.3 Å absorbers. We plot raw object counts in detected electrons as a function of effective rest-frame (peculiar) velocity shift from the centroid of the 2796 Å line. The shading indicates the errors and vertical lines (*Dashed, red*) indicate the expected positions of the MgII lines from the galaxies if they occur at the redshift centroid. We list the quasar name (*Upper left*), and the 3σ upper limit (rest-frame; *Lower right*). The spectra are box-car smoothed by 3 bins. SDSSJ151541.23+334739.4 likely has an absorber but it satisfies $W_{eq}(2796) \leq 0.19$ Å and is therefore not a strong absorber. Note that if the feature at 100 km s^{-1} in SDSSJ111342.42-000730.7 were the 2976 Å line its equivalent width would only be 0.2 Å.

neither the sky nor the quartz lamps provide substantial flux at ∼3100 Å, the data were not flat fielded.

For the detections, we measure the equivalent widths of 2796 Å (only) by fitting Gaussians directly to the spectra and, simultaneously, the background. To estimate the quality of the spectra and the upper limits for the non-detections on an object-by-object basis, we compute a running signal-to-noise estimate of the spectra in the region around the expected Mg II absorption at 2796 Å. Taking a value that is intermediate between the fit widths of our first two detections, we assume an 8-pixel ($\sim$ 1.9 *Å*) line width for each line and compute the total absorption "signal" from within these 8 pixels for each of the the two lines as a function of potential redshift within 300 km s^{-1} of the galaxy center. We take the continuum from the surrounding area. The assumed noise estimate includes contributions from the object counts, the background, readnoise, and an estimate of the error from not flat-fielding the data. We assign upper limits based on the rest-frame equivalent width of a S/N = 3 detection. These results are listed in Table 2.

Figs. 3 - 7 show the raw-count spectra and images for the sample classified by whether we find a significant detection of Mg II within 300 km s^{-1} of the systemic redshift of the galaxy. We only show images of the clear detections and non-detections. Table 2 lists the detection status of the galaxies, as well. Two additional sources, SDSSJ080409.23+385348.8 and SDSSJ081940.82+443649.6, are formally detected at the $\lesssim 3\sigma$ level in the 2796 Å line but at $\gtrsim 3\sigma$ significance in the combination of both lines, although the absorbers are not visually evident in the data. We list these two

Table 2. Galaxy and Absorption Properties

QSO Name	g-r	$M_\star$ (log $M_\odot$)	EW(2796) (Å)	3σ Limit. EW(2796) (Å)	Point Style in Figures
Detections					
SDSSJ091119.16+031152.9	0.692	10.47	0.50	0.23	•
SDSSJ092300.67+075108.2	0.823	10.71	1.93	0.55	•
SDSSJ102847.00+391800.5	0.450	10.15	0.36	0.09	•
SDSSJ114803.17+565411.4	0.770	10.65	1.92	0.30	•
SDSSJ144033.82+044830.9	0.603[a]	10.42	1.24	0.15	•
SDSSJ081420.19+383408.3	0.420	10.01	0.71	0.45	•
Potential Detections[b]					
SDSSJ080409.23+385348.8	0.567	10.50	0.54	0.75	▲
SDSSJ081940.82+443649.6	0.722	10.39	0.40	0.27	▲
Non-Detections of Strong Absorbers					
SDSSJ102751.62+104532.6	0.639	10.54	−−	< 0.23	○
SDSSJ105033.08-001354.8	0.611	10.53	−−	< 0.16	○
SDSSJ111342.42-000730.7	0.825	10.84	−−	< 0.25	○
SDSSJ112613.52+352002.6	0.749	10.50	−−	< 0.20	○
SDSSJ140843.77+004730.4	0.835	10.41	−−	< 0.27	○
SDSSJ151541.23+334739.4	0.678	10.38	−−	< 0.19	○
Weak Non-Detections					
SDSSJ030313.02-001457.4	0.744	10.68	−−	< 1.66	∗
SDSSJ080814.69+475244.6	0.715	10.35	−−	< 0.87	∗
SDSSJ090558.34+504538.0	0.615	10.51	−−	< 0.55	∗
SDSSJ102216.13+621836.7	0.435	10.09	−−	< 0.61	∗
SDSSJ104706.74+375315.4	0.517	10.20	−−	< 1.36	∗
SDSSJ124914.11+392615.0	0.452	10.12	−−	< 0.57	∗

[a]The fainter companion galaxy with a coincident redshift 18.6 h^{-1} kpc from the quasar has $g - r \sim 0.46$.
[b]Significance formally $< 3\sigma$ in single line but $\gtrsim 2.7\sigma$ in both lines; not readily apparent in by-eye examination (see Fig. 7).

TABLE 2
Description of results: (1) SDSS Name of quasar, (2) $g-$ color of the targeted galaxy, (3) stellar mass of the targeted galaxy, (4) equivalent width of 2796 Å Mg II line, (5) expected 2796 Å upper limit for 3σ detection, and (6) point style in Figures.

Table 3. Galaxy Spectral Properties from the SDSS

QSO Name	EW(Hα) (Å)	[NII]/Hα	EW(NaD) (Å)	EW(MgIb) (Å)	EW(Hβ) (Å)	EW(Hδ) (Å)	EW([OII]) (Å)
SDSSJ030313.02-001457.4	1.19±0.20	≫ 0.6	3.46±0.17	7.47±0.34	2.35±0.21	1.58±0.32	−−
SDSSJ080409.23+385348.8	-21.39±0.28	0.34	3.10±0.20	3.62±0.39	-2.68±0.18	2.94±0.42	-1.99±0.30
SDSSJ080814.69+475244.6	-1.00±0.33	2.24	2.56±0.23	6.34±0.50	1.67±0.37	1.31±0.35	-6.52±0.55
SDSSJ081420.19+383408.3	-9.67±0.23	0.45	1.29±0.26	3.65±0.51	-0.97±0.15	3.62±0.40	-3.21±0.35
SDSSJ081940.82+443649.6	-1.10±0.15	2.18	4.48±0.23	7.13±0.64	1.89±0.30	1.57±0.32	-3.27±0.51
SDSSJ090558.34+504538.0	-1.86±0.33	1.21	2.99±0.39	10.43±1.50	3.04±0.90	3.38±1.78	-3.12±1.63
SDSSJ091119.16+031152.9	-2.09±0.14	1.25	4.26±0.20	4.87±0.46	2.84±0.48	1.17±0.57	0.07±0.20
SDSSJ092300.67+075108.2	-0.06±0.08	≫ 0.6	5.77±0.21	8.35±0.69	3.54±0.46	2.48±0.72	-2.68±0.88
SDSSJ102216.13+621836.7	-19.68±0.48	0.35	2.23±0.39	5.07±1.44	-4.36±0.38	6.71±1.12	-7.59±0.79
SDSSJ102751.62+104532.6	-1.74±0.28	1.80	2.35±0.38	7.40±0.70	2.64±0.57	-0.07±0.25	-3.09±0.85
SDSSJ102847.00+391800.5	-31.35±0.49	0.35	1.86±0.37	1.80±0.38	-5.25±0.27	0.17±0.13	-7.54±0.45
SDSSJ104706.74+375315.4	-24.59±0.50	0.76	0.33±0.20	3.89±0.73	-13.04±0.95	-0.24±0.22	-1.40±0.27
SDSSJ105033.08-001354.8	-6.32±0.23	0.55	3.38±0.18	5.92±0.43	0.88±0.15	2.10±0.40	-1.26±0.28
SDSSJ111342.42-000730.7	0.14±0.05	≫ 0.6	6.11±0.21	9.16±0.39	2.12±0.30	1.07±0.27	5.93±2.27
SDSSJ112613.52+352002.6	-1.31±1.14	−−	4.10±0.25	8.45±0.53	2.96±0.37	1.40±0.38	13.10±21.89
SDSSJ114803.17+565411.4	-0.85±0.23	3.44	6.71±0.29	8.47±0.74	-0.16±0.13	-0.21±0.39	-7.26±1.12
SDSSJ124914.11+392615.0	-53.00±5.00	−−	−−	1.87±0.37	-12.04±0.30	-0.50±0.16	-12.46±0.37
SDSSJ140843.77+004730.4	-0.36±0.15	0.6	4.63±0.35	7.38±0.79	2.25±0.44	0.49±0.40	1.89±1.37
SDSSJ144033.82+044830.9	-6.17±0.17	0.51	2.65±0.19	5.09±0.41	-0.46±0.11	2.62±0.36	-3.02±0.45
SDSSJ151541.23+334739.4	-6.95±0.24	0.75	3.97±0.22	4.78±0.41	2.25±0.44	2.97±0.38	-2.29±0.25

TABLE 3
SDSS SpecLine properties of targeted galaxies: (1) SDSS Name of quasar, (2) Hα equivalent width, (3) ratio of [NII] 6586 Å line to Hα, (4) - (8) equivalent widths of Na I D, Mg I b, Hβ, Hδ, and [OII].

sources as "probable detections." Fig. 8 describes the redshifts and quasar magnitudes for the observations, illustrating that the significant non-detections — the most stringent requirements on the spectra — are much more readily obtained at relatively high redshifts, as expected from the sharp atmospheric cutoff near $3050 - 3100$ Å.

If we increase the assumed width used to calculate the upper limits from 8 to 12 pixels, the upper limits increase by ∼20%, pushing SDSSJ111342.42-000730.7 and SDSSJ140843.77+004730.4 below the limit. If a small feature at ∼100 km s^{-1} in SDSSJ111342.42-000730.7 were real and the blue line were masked by the unrelated absorption feature at 900 km/s, its $W_{eq}(2796)$ would still be only be 0.2 Å, so it is not a strong absorber. SDSSJ140843.77+004730.4 is a potential (barely) 3σ detection, but it would be at ∼-316 km s^{-1}, which is probably unphysical.

Most of the galaxies do not have evident faint companions closer to the quasar. However, the strong absorber in SDSSJ144033.82+044830.9 has a companion with $m_r = 18.1$ and $M_R = -19.8$ at a projected 18.6 h^{-1} kpc from the quasar. Although its redshift was not acquired as part of the SDSS, we obtained a spectrum with the Keck telescope on 2009 January 25, measuring $z = 0.1128$ after correcting to the local standard of rest using the IRAF tast RVCORRECT. This redshift is within the measurement error of the redshift for the primary galaxy. The companion is even bluer than the luminous galaxy, however, with $g - r \sim 0.46$. Both the companion and the Mg II-absorbing gas are almost certainly within the dark matter halo of the more luminous galaxy. Thus, they are all likely associated with the potential fuel for star formation in the outskirts of the central galaxy.

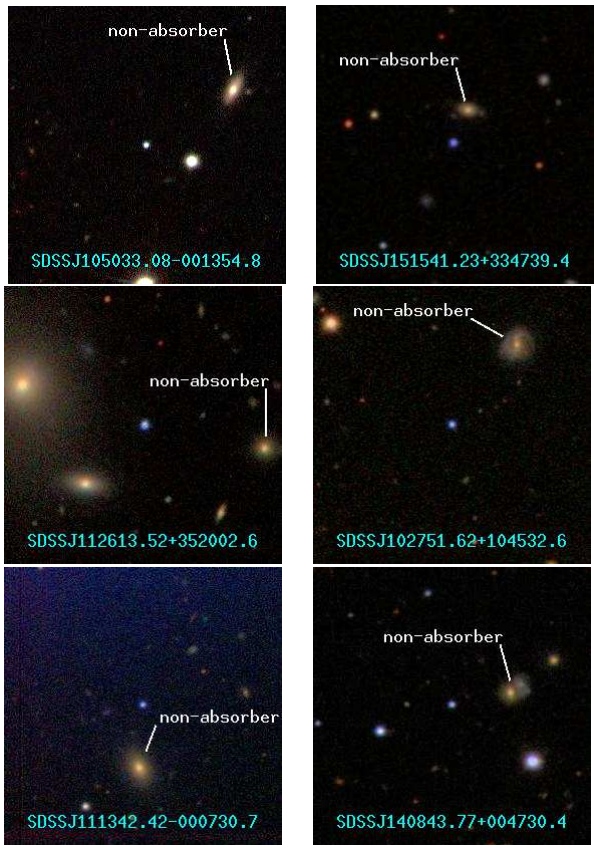

FIG. 6.— The galaxies that were not detected. We show SDSS images of the quasars and galaxies with ≤ 0.3 Å upper limits that are non-detections of strong absorbers. The central object is the quasar and the images are 40″ on a side, corresponding (*Left to right*) to 59, 59, 57, 56, 56,, and 58 h^{-1} kpc, respectively.

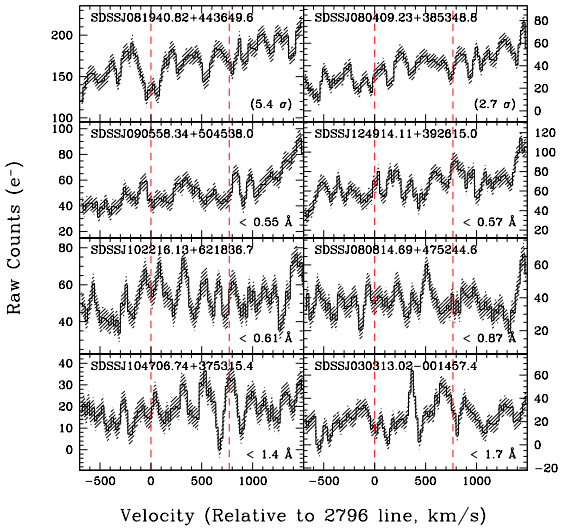

FIG. 7.— The potential detections (*Top row*) and weaker non-detections that are inconclusive with respect to strong (> 0.3 Å) absorbers. We plot raw object counts in detected electrons as a function of effective rest-frame (peculiar) velocity shift from the centroid of the 2796 Å line. Shading indicates the errors and vertical lines (*Dashed, red*) indicate the expected positions of the MgII lines from the galaxies if they occur at the redshift centroid. We list a short-hand version of the quasar name (*Upper left*), and either the significance of the potential detection or the 3σ upper limit of non-detection (rest-frame; *Lower right*). The spectra are box-car smoothed by 3 bins.

3. RESULTS

To explore the characteristics of "strong" [$W_{eq}(2796) > 0.3$Å] Mg II absorbers in the local universe, we compare the properties of the detected absorbers with the non-absorbers and the full volume-limited sample.

Table 1 and Fig. 9 show properties of the samples, including rest-frame colors, luminosities, and stellar masses from the kcorrect fitting results distributed with the NYU-VAGC (Blanton et al. 2005b; Blanton & Roweis 2007). The solid lines show the full volume-limited samples, where measurements are available, and the filled histograms show the probed galaxies. The detected Mg II absorbers span the full range of colors and $W_{eq}(H\alpha)$, and most of the range of luminosities and stellar masses of the sample. For this small sample of six absorbers, K-S tests reveal no significant differences between the distributions of the absorbers and the full sample. However, we note that K-S tests are not uniformly sensitive to all kinds of trends.

K-S tests reveal no evident unfairness in the sampling of parameter space except in Hα. The 20 sampled galaxies fall preferentially at somewhat smaller $W_{eq}(H\alpha)$ (stronger emission) than the full volume-limited sample ($P_{K-S} = 0.05$), with an average of -9.4 Å for the 20 probed systems as compared with -7 Å for the full volume-limited sample.

3.1. *Star formation*

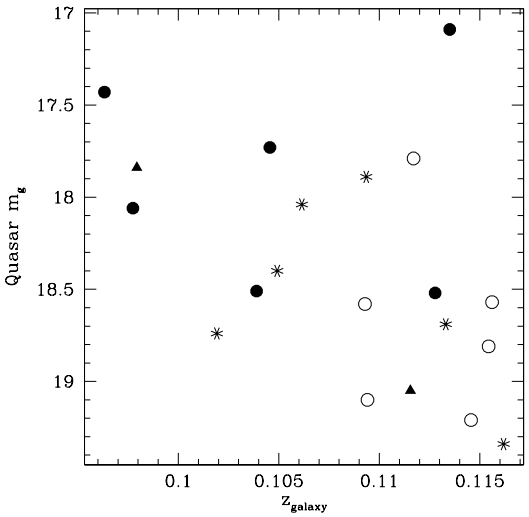

FIG. 8.— Absorber result as a function of galaxy redshift and quasar g-band apparent magnitude. Using data from Table b, we plot detections of strong (> 0.3 Å) absorbers (*Filled circles*), non-detections of strong absorbers (*Open circles*), potential strong absorbers (*Filled triangles*), and weak non-detections (*Stars*) which could be strong absorbers but not very strong absorbers (see Table b). The significant non-detections of strong absorbers, which require the best data quality, cluster at higher redshifts because of atmospheric extinction.

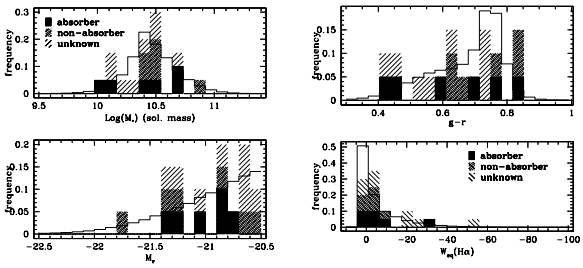

FIG. 9.— Properties of the targeted galaxies in the context of the volume-limited SDSS sample. When they are available, we show the approximate stellar masses (*Top left*), r-band absolute magnitudes (*Bottom left*), $g-r$ colors (*Top right*), and $W_{eq}(H\alpha)$ (*Bottom right*) for the full volume-limited $M_r - 5\log h \leq -20.5$ sample (*solid line*), the galaxies we have already targeted. We show the ambiguous potential detections and weak non-detections (*lightest shading*) the strong non-detections (*medium shading*) and the detections(*darkest shading*). Here, we plot the luminous galaxy for the absorber SDSSJ144033.82+044830.9 ($\log M_\star = 10.42, M_r = -21.3, g-r = 0.603$), although its bluer and fainter minor companion is the likely source of at least some of the Mg II absorption. The histograms for the targeted galaxies are non-overlapping.

The data suggest, but do not conclusively establish, the existence of trends in Mg II properties and star-forming properties. The most striking potential color dependence on absorption characteristics is that confirmed non-strong-absorbers (*Medium shading*) are green or red but not blue. Although the trend does not yield a low K-S probability, there is a somewhat significant effect in the measured average $g-r$ color. The average color for the full sample is $< g-r >= 0.643$, while it is 0.723 for the non-detections of strong absorbers. If we randomly draw six $g-r$ colors at random from the full volume-limited DR6 sample 10,000 times, the average is only as red as 0.723 by chance 15% of the time, a $\sim 1\sigma$ result. A larger sample is crucial for confirming this possible trend. For

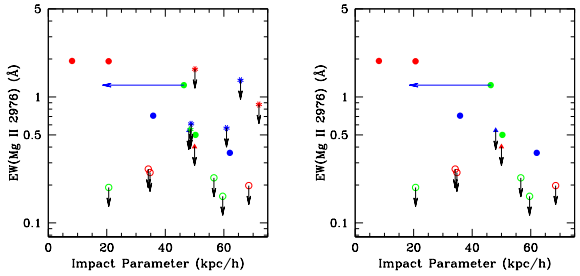

FIG. 10.— Mg II absorption as a function of impact parameter from our volume-limited SDSS sample. (*Left*) We plot the measured $W_{eq}(2796)$ or upper limit of the 2796 Å absorption line as function of impact parameter between the quasar and the targeted galaxy. Points are segregated based on color (*Blue:* $g-r < 0.6$, *green:* $0.6 < g-r < 0.7$, *or red:* $g-r > 0.7$) and on the presence or absence of 2796 Å absorption as described in Table b. (*Right*) We show the same figure without the ambiguous, lower S/N spectra. SDSSJ144033.82+044830.9 is plotted at the luminous galaxy's position, but with an arrow pointing to the position of its confirmed minor companion.

$W_{eq}(H\alpha)$, the non-absorbers are relatively weaker star-formers, but at lower significance. The average for the full sample is $W_{eq}(H\alpha) = -9.4$ Å while it is -2.7 Å for the 6 non-absorbers, but an average this large happens by chance 28% of the time.

Fig. 10 depicts the relationships between the colors, impact parameters, and strengths of the absorbers. We plot $W_{eq}(2796)$ as a function of impact parameter for galaxies with different absorption status, also color-coding based on $g-r$ color, where blue points have $g-r < 0.6$, green points have $0.6 < g-r < 0.7$ and red points have $g-r > 0.7$. In the right-hand side of the figure, we eliminate the most ambiguous points to give a clearer view of the possible trends.

Among the absorbers, the tendency for stronger absorbers to appear at smaller impact parameters, as noted by Steidel (1995) and more recently Zibetti et al. (2007), is also suggested by our data. All of the bluest galaxies are either strong absorbers or inconclusive, although the "green" galaxies can be non-absorbers. The confirmed absorbers at higher impact parameters are all blue. Furthermore, the only definitive red absorbers are at very small impact parameter (≤ 20 h^{-1} kpc), although one possible red absorber (SDSSJ081940.82+443649.6) lies at 48 h^{-1} kpc. We note that the red absorbers all exhibit some emission-line flux in their spectra, with [NII]/Hα flux ratios characteristic of LINERs; these red, emitting galaxies are very common (e.g., Yan et al. 2006; Graves et al. 2007).

Overall, the data are suggestive that in the low-z universe, the absorption and covering fraction may depend on the star-forming properties of galaxies. Specifically, non-absorbers may be primarily green or red galaxies, and red absorbers may favor lower impact parameters. These relationships are in broad agreement with the possibility that a gas halo is required to replenish continuously star-forming galaxies (e.g., Larson et al. 1980) and with the statistical finding of Zibetti et al. (2007) that stronger Mg II absorbers in SDSS quasars are surrounded by bluer light distributions. Confirming these results would require better sampling by color that includes more blue galaxies at lower impact parameters and more red galaxies at higher impact parameters.

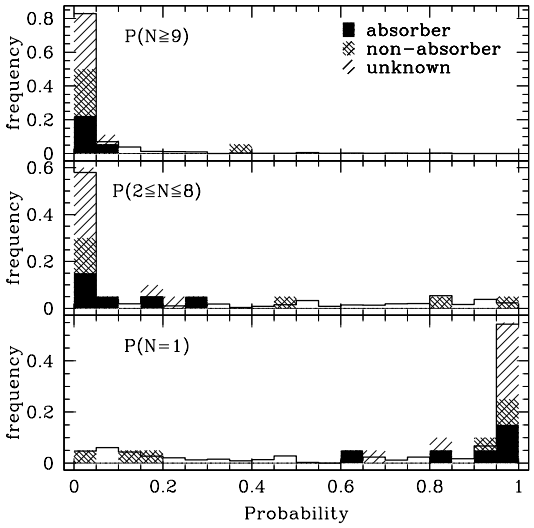

FIG. 11.— The environmental properties of the targeted galaxies in the context of the volume-limited SDSS sample. We use numerical simulations to estimate the probability that the galaxies are (*Bottom*) alone in their dark matter halos with respect to other luminous galaxies, P(N = 1), (*Middle*) in systems with 2-8 luminous members, P(2 ≤ N ≤ 9), or (*Top*) in dense systems with ≥ 9 members P(N ≥ 9). The graph types follow Fig. 9. Here, we plot the results for luminous galaxy near the absorber SDSSJ144033.82+044830.9, with P(N = 1) = 0.93, P(2 ≤ N ≤ 8) = 0.06, and P(N ≥ 9) = 0.009.

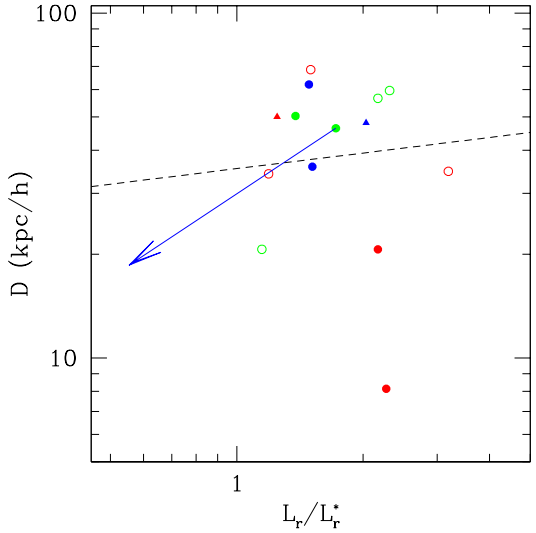

FIG. 12.— Absorption status as a function of galaxy luminosity and impact parameter. We plot the more reliable absorbers (*Filled circles*), non-absorbers (*Open circles*), and potential or likely absorbers (*Filled triangles*) as a function of absolute *r*-band luminosity and impact parameter, following Steidel (1995). We plot SDSSJ144033.82+044830.9 at the luminous galaxy's position, but with an arrow pointing to the position of its confirmed minor companion. Results differ dramatically from the intermediate-redshift Steidel study in which galaxies above the line were essentially all non-absorbers and galaxies below the line were nearly all absorbers. The points are color-coded as in Fig. 10.

3.2. *Environment*

A modification of the method described in Barton et al. (2007) allows us to characterize the environments of the galaxies in the volume-limited sample objectively, by comparison to a cosmological dark matter simulation (Zentner & Bullock 2003; Zentner et al. 2005; Allgood et al. 2006). Using number-density matching to match the $M_r + 5\log h \leq -20.5$ sample to dark matter halos in the simulation with circular speeds ≥ 240 km s^{-1}, we create an artificial redshift survey with the simulation and bin model halos by the distance to the nearest massive neighbor within 1000 km s^{-1}, D_N, and the number of neighbors it has in total within 700 h^{-1} kpc and 1000 km s^{-1}, N_{700}. Then, for each bin in D_N and N_{700}, we compute the probability that a halo in that bin is alone with respect to other halos in the sample, P(N=1), the probability that a galaxy in each bin has 1-7 companions, P(2 ≤ N ≤ 8), and the probability that it resides in a cluster with ≥ 8 other halos, P(N≥ 9). For each galaxy in the volume-limited SDSS sample, we measure D_N and N_{700} from the data then compute P(N = 1), P(2 ≤ N ≤ 8), and P(N≥ 9) using the corresponding bin in the simulation.

Fig. 11 shows the distributions of these probabilities for the portion of the full volume-limited sample that falls into relatively complete regions of the SDSS. Again, because of the small sample sizes, K-S tests reveal few significant trends; comparing the distribution of P(2 ≤ N ≤ 8) shows that the sample of 20 galaxies probed this study as a whole differs at a minor level from the population at large at ($P_{K-S} = 0.10$).

As the distribution of P(N=1) shows, most of the galaxies in the volume-limited sample are isolated by these criteria, primarily because the magnitude limit of the sample is quite luminous. Nonetheless, the detected absorbers are even more isolated than the population at large, with probabilities P(N = 1) ≳60%. We note that although 71% of the galaxies in the full sample fall into this regime, the probability that all 6 absorbers fall into the P(N=1) > 0.6 regime by chance is still modest (12%). The possible environmental effects are further accentuated by the results for the non-absorbers. Only 18.5% of the full volume-limited sample have P(N=1)< 0.20%, while 3/6 of the non-absorbers are in this category. The binomial probability that 3 or more would fall into the P(N=1) < 0.2 regime by chance is ∼ 8%. Taken together, the two constitute a ≳2σ result, although this significance is somewhat overstated because of the *a posteriori* nature of the estimate. Thus, the data suggest that absorbers tend to be isolated and that non-absorbers are more likely to have companions.

This result is broadly consistent with "strangulation," or the stripping of a galaxy's outer gas halo when it falls into a denser system (e.g., Larson et al. 1980). When galaxies become substructure in a larger system, this stripping eventually cuts off the fuel for star formation, explaining why galaxies in denser environments gradually turn red. As the data suggest, these galaxies in denser environments may be less likely to exhibit Mg II absorption.

3.3. *Covering fraction*

The covering fraction of Mg II absorption is a fundamental property that describes the statistical amount of Mg II-absorbing gas around typical galaxies; it provides an important constraint on the behavior of gas in models (e.g., Kaufmann et al. 2009; Kacprzak et al. 2009). Hydrodynamic simulations predict a range of Mg II covering fractions depending in detail on the temperature

and entropy of the gas. For example, Kaufmann et al. (2009) show that a change in temperature of a factor of two can change the Mg II covering fraction by a factor of ∼30. Thus, an accurate and unbiased measure of this fraction around a uniform set of galaxies, even with accuracy that is within a factor of a few, is a strong constraint on the nature of halo gas in galaxies.

Several empirical studies explore models in which the size of the absorbing gas "halo" scales with galaxy luminosity (Bowen et al. 1995; Steidel 1995; Guillemin & Bergeron 1997; Kacprzak et al. 2008). Because our luminosity range is extremely small, we primarily constrain the gas "halo" near $L_r^\star$ (∼-20.44; Blanton et al. 2003). We show the relationship between absorber status, impact parameter, and galaxy luminosity in Fig. 12. The dotted line is the line from Steidel (1995), albeit for K-band luminosities. In their study, almost all of the intermediate-redshift sample are non-absorbers above the line, while below the line, their galaxies are almost exclusively absorbers. Our data are very inconsistent with this picture, with absorbers and non-absorbers falling above and below the line in nearly equal numbers. Furthermore, because one of the galaxies with the largest impact parameters exhibits Mg II absorption, our only constraint on the gas halo radius is that $R \gtrsim 62$ h^{-1} kpc near $L_r^\star$. This inconsistency could arise from selection effects, redshift differences, or by chance.

Because of the non-uniformity in the quality of the spectra, we are forced to cull our sample in order to yield an estimate of f_c, the covering fraction of gas or the fraction of sightlines through the gas "halo" that will exhibit "strong" [$W_{eq}(2796) \geq 0.3$ Å] absorption (Steidel 1995). To measure the covering fraction of strong absorbers, we exclude all spectra from Table 2 with 3σ upper limits > 0.3 Å, which must necessarily exclude the strong absorbers SDSSJ092300.67+075108.1 and SDSSJ081420.19+383408.3, and could exclude SDSSJ114803.17+565411.4, with an upper limit equivalent to 0.3 Å. These lower-S/N quasar spectra can reveal strong absorbers but cannot detect strong non-absorbers; thus, their inclusion could bias the sample toward finding more absorbers. We also exclude SDSSJ144033.82+044830.9 because of its minor companion ($M_R = -19.8$) closer to the quasar. Unfortunately, SDSSJ081940.82+443649 is an ambiguous case, as the formal 3σ limit is < 0.27 Å but the detection remains relatively tentative. Depending on whether we include or exclude J114803 and/or J144033, we estimate an overall covering fraction within ∼75 h^{-1} kpc of $f_c = 2/8-4/10 = 0.25 - 0.4$. If we consider only those probes within the traditional ∼35 h^{-1} kpc, our statistics become sparse, yielding an estimate of $f_c = 0/3 - 1/4 = 0 - 0.25$, depending on how we treat SDSSJ114803.17+565411.4.

The early studies of Mg II absorption suggested that f_c is near unity. In our study, several absorbers have larger impact parameters than some of the non-absorbers. Our low-z data are inconsistent with a gas covering fraction of 1. Some previous studies agree with our results, finding gas covering fractions well below 1 (Bechtold & Ellingson 1992; Bowen et al. 1995; Churchill et al. 2005; Tripp & Bowen 2005; Kacprzak et al. 2008), while others favor fractions much closer to 0.8-1 (Steidel 1995; Chen & Tinker 2008). Broadly speaking, "reverse" studies such as ours, that identify galaxies first and then explore Mg II properties, may measure lower covering fractions. The discrepancies among studies could also result from dramatic differences in redshift, halo mass, and galaxy properties for the systems that are probed; both factors are likely to make a difference (e.g., Bowen et al. 1995; Tinker & Chen 2008).

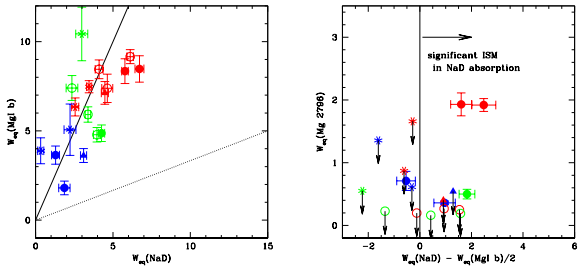

FIG. 13.— The ISM as diagnosed by NaD line strength. Following Rupke et al. (2005a), we probe the ISM of the targeted galaxies "down the barrel," using the SDSS spectra of the galaxies themselves. (*Left*) We plot W_{eq}(NaD) vs. W_{eq}(MgI b) for the galaxies in this study. The solid line shows the expected relationship for purely stellar NaD: W_{eq}(NaD) = 0.5 W_{eq}(MgI b); the dashed line marks the region where winds are prevalent (Rupke et al. 2005a,b). Thus, galaxies closer to the right of the solid line are more likely to be ISM dominated in NaD. (*Right*) We also plot W_{eq}(2796) as a function of W_{eq}(NaD) corrected for stellar absorption; the strongest confirmed galaxy halo absorbers (*Red points*) have spectra that suggest a significant contribution of the to NaD line. We exclude SDSSJ144033.82+044830.9 because of its closer faint companion; point styles follow Fig 10.

3.4. *Other properties of the interstellar medium*

The possible color dependence noted here and elsewhere and the environmental dependence our data support the expectation that there are fundamental relationships between the abundance of halo gas in a galaxy and its star-forming properties. The Mg II halo gas may also relate to the interstellar medium (ISM), as observed "down-the-barrel" in galaxy spectra. The Na I D absorption-line doublet (λ5890,5896 Å) is a sensitive, well-studied ISM diagnostic that falls into the optical regime at low redshift. Unfortunately, it suffers from contamination by starlight. Nonetheless, high-resolution studies of the doublet show clear-cut winds in the Na I D line in rapidly star-forming ultraluminous infrared galaxies (Martin 2005; Rupke et al. 2005a,b).

The contamination from a stellar component to the Na I D line can be estimated from the equivalent width of the Mg I b triplet (λ5167,5173,5185 Å). Various authors assume a stellar contribution to W_{eq}(NaD) of $(\frac{1}{3} - \frac{1}{2})\times$ W_{eq}(MgI b). In Fig. 13, we plot W_{eq}(MgI b) as a function of W_{eq}(NaD). Following Rupke et al. (2005a), we plot the line W_{eq}(NaD) = 0.5 W_{eq}(MgI b) (*Solid line*); points further to the right of the solid line are more likely to have contributions from the ISM to the Na I D absorption. The dotted line is the approximate location of starbursting galaxies with strong winds observed in the Na I D feature for the Rupke et al. (2005a) sample. We code the points based on Mg II absorption status in the halo of the galaxy. None of the DR6 -20.5 sample galaxies observed thus far lie in the strong-wind regime. Nonetheless, there is a suggestion that the galaxies with Mg II halo absorption lie at relatively large W_{eq}(NaD)-to-W_{eq}(MgI b) ratio, as illustrated by the right-hand side

of the plot. All of the red absorbers have relatively strong Na I D absorption given their W_{eq}(MgI b). In fact, only one absorber lies at W_{eq}(MgI b)$> 0.5W_{eq}$(NaD)and it is blue (SDSSJ081420.19+383408.3). Perhaps red galaxies with halo Mg II must actually be either very dusty or gas-rich enough to exhibit significant Na I D from the ISM which has not yet resumed star formation. Blue galaxies with little interstellar Na I D could be systems at the end of their star-forming cycle that have used up or cleared out their low impact parameter Na I D gas, but have retained their outer halo gas; the relatively strong Balmer absorption in SDSSJ081420.19+383408.3 [$W_{eq}(H\delta) = 3.6$ Å] supports this hypothesis.

4. CONCLUSIONS

We use ground-based spectroscopy with LRIS-B on the Keck I telescope to evaluate the Mg II absorption characteristics of a sample of $\sim L^{\star}$ galaxies selected as cleanly as possible from a volume-limited subsample to $M_r + 5\log h \gtrsim -20.5$ of the SDSS DR6 Value Added Galaxy Catalog (Blanton et al. 2003). We target 20 systems, achieving a range in the quality of spectral observations that reveals 6 "strong" [$W_{eq}(2796) > 0.3$ Å] absorbers and 6 non-absorbers. We find the following:

1. Ground-based observations of Mg II absorption are possible — with relatively low S/N ratio — to redshifts as low as $z \sim 0.1$ with modest amounts of observing time.

2. The overall covering fraction, f_c, of gas capable of creating strong (≥ 0.3 Å) Mg II absorption must be < 1 at $z \sim 0.1$, broadly consistent with some previous studies. Even inside the traditional absorption halo radius of $\sim$35 h^{-1} kpc, the covering fraction of strong absorption is < 1, with a naive estimate of $f_c \lesssim 0.25$.

3. The Mg II detection in the quasar with the largest impact parameter lies 62 h^{-1} kpc from the center of the associated galaxy. Thus, at least in rapidly star-forming $z \sim 0.1$ galaxies, strong, but possibly unfilled, Mg II absorption gas halos can extend to at least this distance from a luminous galaxy.

4. The data suggest, at the $\lesssim 2\sigma$ significance level, that the Mg II absorption properties of the outer halos of galaxies may depend on the larger-scale environment of the absorbing galaxy. Absorbers appear to favor low-density environments, while non-absorbers show a possible preference for denser regions. This result is consistent with "strangulation" models in which satellite galaxies are red because their outer gas halos are stripped when they become substructure.

5. The relationships between galaxy color, impact parameter, and absorbing halo $W_{eq}(2796)$ are consistent with a model in which red galaxies with Mg II absorption are typically LINERs which are observed at smaller impact parameters. Blue galaxies are possible Mg II absorbers to very large impact parameters (at least 62 h^{-1} kpc); in fact, all of the bluest galaxies in this study are either strong absorbers or inconclusive. These color trends are consistent with the results from statistical image-stacking studies (Zibetti et al. 2007), and with the broad expectations of theoretical models.

We gratefully acknowledge the Sloan Digital Sky Survey and the hard work of M. Blanton and collaborators to create the NYU-Value Added Galaxy Catalog. We thank James Bullock, Andrew Zentner, Risa Wechsler, David Tytler, Aaron Barth, Glenn Kacprzak, and Taotao Fang for assistance, advice and support. EJB and JC acknowledge generous support from the Center for Cosmology at UC Irvine and JC gratefully acknowledges support from Gary McCue. The authors wish to recognize and acknowledge the very significant cultural role and reverence that the summit of Mauna Kea has always had within the indigenous Hawaiian community. We are most fortunate to have the opportunity to conduct observations from this mountain.

Funding for the Sloan Digital Sky Survey (SDSS) and SDSS-II has been provided by the Alfred P. Sloan Foundation, the Participating Institutions, the National Science Foundation, the U.S. Department of Energy, the National Aeronautics and Space Administration, the Japanese Monbukagakusho, and the Max Planck Society, and the Higher Education Funding Council for England. The SDSS Web site is http://www.sdss.org/. The SDSS is managed by the Astrophysical Research Consortium (ARC) for the Participating Institutions. The Participating Institutions are the American Museum of Natural History, Astrophysical Institute Potsdam, University of Basel, University of Cambridge, Case Western Reserve University, The University of Chicago, Drexel University, Fermilab, the Institute for Advanced Study, the Japan Participation Group, The Johns Hopkins University, the Joint Institute for Nuclear Astrophysics, the Kavli Institute for Particle Astrophysics and Cosmology, the Korean Scientist Group, the Chinese Academy of Sciences (LAMOST), Los Alamos National Laboratory, the Max-Planck-Institute for Astronomy (MPIA), the Max-Planck-Institute for Astrophysics (MPA), New Mexico State University, Ohio State University, University of Pittsburgh, University of Portsmouth, Princeton University, the United States Naval Observatory, and the University of Washington.

REFERENCES

Adelman-McCarthy, J., Agueros, M. A., Allam, S.S., et al. 2006, ApJS, 162, 38
Adelman-McCarthy, J. K., et al. 2008, ApJS, 175, 297
Allgood, B., Flores, R. A., Primack, J. R., Kravtsov, A. V., Wechsler, R. H., Faltenbacher, A., & Bullock, J. S. 2006, MNRAS, 367, 1781
Barton, E. J., Arnold, J. A., Zentner, A. R., Bullock, J. S., & Wechsler, R. H. 2007, ApJ, 671, 1538
Bechtold, J., & Ellingson, E. 1992, ApJ, 396, 20
Bergeron, J., & Boissé, P. 1991, A&A, 243, 344
Blanton, M. R., et al. 2003, ApJ, 594, 186
Blanton, M. R., Eisenstein, D., Hogg, D. W., Schlegel, D. J., & Brinkmann, J. 2005, ApJ, 629, 143
Blanton, M. R., et al. 2005, AJ, 129, 2562
Blanton, M. R., & Roweis, S. 2007, AJ, 133, 734

Bouché, N., Murphy, M. T., Péroux, C., Csabai, I., & Wild, V. 2006, MNRAS, 371, 495
Bowen, D. V., Blades, J. C., & Pettini, M. 1995, ApJ, 448, 634
Chen, H.-W., Lanzetta, K. M., & Webb, J. K. 2001, ApJ, 556, 158
Chen, H.-W., & Tinker, J. L. 2008, ApJ, 687, 745
Churchill, C. W., Steidel, C. C., & Vogt, S. S. 1996, ApJ, 471, 164
Churchill, C. W., Rigby, J. R., Charlton, J. C., & Vogt, S. S. 1999, ApJS, 120, 51
Churchill, C. W., Kacprzak, G. G., & Steidel, C. C. 2005, IAU Colloq. 199: Probing Galaxies through Quasar Absorption Lines, 24
Dressler, A. 1980, ApJ, 236, 351
Graves, G. J., Faber, S. M., Schiavon, R. P., & Yan, R. 2007, ApJ, 671, 243
Guillemin, P., & Bergeron, J. 1997, A&A, 328, 499
Gunn, J. E., & Gott, J. R., III 1972, ApJ, 176, 10
Kacprzak, G. G., Churchill, C. W., Steidel, C. C., Murphy, M. T., & Evans, J. L. 2007, ApJ, 662, 909
Kacprzak, G. G., Churchill, C. W., Steidel, C. C., & Murphy, M. T. 2008, AJ, 135, 922
Kacprzak, G. G., Churchill, C. W., Steidel, C. C., Klypin, A., & Murphy, M. T., 2009, submitted
Kaufmann, T., Bullock, J. S., Maller, A. H., Fang, T., & Wadsley, J. 2009, MNRAS, 396, 191
Kawata, D., & Mulchaey, J. S. 2008, ApJ, 672, L103
Larson, R. B., Tinsley, B. M., & Caldwell, C. N. 1980, ApJ, 237, 692
Maller, A. H., & Bullock, J. S. 2004, MNRAS, 355, 694
Martin, C. L. 2005, ApJ, 621, 227
McCarthy, J. K., et al. 1998, Proc. SPIE, 3355, 81
Moore, B., Katz, N., Lake, G., Dressler, A., & Oemler, A. 1996, Natur e, 379, 613
Nestor, D. B., Turnshek, D. A., & Rao, S. M. 2005, ApJ, 628, 637
Nestor, D. B., Turnshek, D. A., & Rao, S. M. 2006, ApJ, 643, 75
Nestor, D. B., Turnshek, D. A., Rao, S. M., & Quider, A. M. 2007, ApJ, 658, 185
Oke, J. B., et al. 1995, PASP, 107, 375
Postman, M., & Geller, M. J. 1984, ApJ, 281, 95
Rupke, D. S., Veilleux, S., & Sanders, D. B. 2005a, ApJS, 160, 87
Rupke, D. S., Veilleux, S., & Sanders, D. B. 2005b, ApJS, 160, 115
Schneider, D. P., et al. 2007, AJ, 134, 102
Steidel, C. C., & Sargent, W. L. W. 1992, ApJS, 80, 1
Steidel, C. C., Dickinson, M., & Persson, S. E. 1994, ApJ, 437, L75
Steidel, C. C. 1995, QSO Absorption Lines, 139
Tinker, J. L., & Chen, H.-W. 2008, ApJ, 679, 1218
Tripp, T. M., & Bowen, D. V. 2005, IAU Colloq. 199: Probing Galaxies through Quasar Absorption Lines, 5
Yan, R., Newman, J. A., Faber, S. M., Konidaris, N., Koo, D., & Davis, M. 2006, ApJ, 648, 281
Zentner, A. R., & Bullock, J. S. 2003, ApJ, 598, 49
Zentner, A. R., Berlind, A. A., Bullock, J. S., Kravtsov, A. V., & Wechsler, R. H. 2005, ApJ, 624, 505
Zibetti, S., Ménard, B., Nestor, D., & Turnshek, D. 2005, ApJ, 631, L105
Zibetti, S., Ménard, B., Nestor, D. B., Quider, A. M., Rao, S. M., & Turnshek, D. A. 2007, ApJ, 658, 161